Electroluminescence image-based defective photovoltaic (solar) cell detection using a modified deep convolutional neural network

Hiren MEWADA[1,a *], L. SYAMSUNDAR[2,b], Hiren Kumar THAKKAR[3,c] and Miral DESAI[4,d]

[1]Electrical Engineering Department, Prince Mohammad Bin Fahd University, P.O. Box 1664, Al Khobar 31952, Kingdom of Saudi Arabia

[2]Mechanical Engineering Department, Prince Mohammad Bin Fahd University, P.O. Box 1664, Al Khobar 31952, Kingdom of Saudi Arabia

[3]Department of Computer Science and Engineering, School of Technology, Pandit Deendayal Energy University, Gandhinagar, Gujarat, India, 382421

[4]V. T. Patel Department of Electronics and Communication Engineering, Chandubhai S Patel Institute of Technology, Charotar University of Science and Technology, Changa, Gujarat, India

[a]hmewada@pmu.edu.sa, [b]slingala@pmu.edu.sa, [c]hiren.pdeu@gmail.com, [d]miraldesai.ec@charusat.ac.in

Keywords: Renewable Energy, Photovoltaic Solar Panels, Deep Convolution Neural Network, Image Classification

Abstract. Electroluminescence (EL) imaging of photovoltaic solar cells can detect and classify solar panel faults. This method allows technicians and manufacturers to identify defective panels that may affect performance and longevity. However, noise in EL images and solar cell silicon granularity make this process difficult. The paper presents an automated deep-learning framework to identify faulty and normal solar cells from images. Xception, a popular CNN network, is modified to reduce complexity and solve overfitting issues. Few separable convolution layers were removed from the original Xception network, and lateral dropout layers were added. The proposed deep CNN is tested on ELVP. To balance two classes, images are augmented with two rotations and dimensional shifting. Finally, the proposed model is compared to a pretrained CNN network and leading methods. The quantitative analysis showed that the model performed better than previous methods, with 94.382% accuracy, 92% precision, 95.12% recall rate, and 93.53% F1 score. Module fault identification helps with maintenance planning. Solar energy's widespread adoption and growth as a renewable and sustainable power source may result.

Introduction

Solar power has grown in popularity as a renewable energy source. Over the past decade, massive solar power plants worldwide have enabled large-scale solar energy component production. The photovoltaic (PV) module is essential to solar power. How well solar energy systems work depends on solar module efficiency. Crystalline silicon (c-Si) photovoltaic (PV) modules are the most popular due to their low cost per watt and well-established manufacturing process. Tang et al. [1], say this technology accounts for 97% of monocrystalline and polycrystalline module sales.

Solar panel fault classification is necessary for several reasons. First, a solar panel fault can reduce energy output. It streamlines maintenance planning and resource allocation. Technicians can optimize their efforts and address critical issues quickly by categorizing and prioritizing faults by severity and impact. Additionally, fault classification in electroluminescent solar panels has helped develop predictive maintenance strategies. By analyzing historical fault data and understanding patterns and trends, predictive models can predict and prevent faults. In solar panel manufacturing, fault classification is crucial to quality control. Before deployment, manufacturers can identify and classify panel defects using imaging. This ensures customers receive high-quality

panels, improving satisfaction and reducing the risk of premature failure or performance degradation.

These solar panel faults can be identified using I-V curve measurements, thermal-infrared imaging (IR), and electroluminescence (EL) imaging. The I-V curve approach utilizes graphs to display PV module voltage and current output under specific radiation conditions. While the I-V curve can show module status, it cannot identify faulty cells or their locations. Using infrared imaging to monitor solar modules and cells is another popular method. An open circuit can cool a place, while a large current can heat it. IR imaging can detect dead cells, hot spots, and short circuits. However, thermal cameras' low resolution prevents them from detecting microcracks [2]. Such issues can be resolved via EL imaging. One nondestructive way to detect PV module defects is with an EL test. EL imaging can discover faulty cells and regions with ease and provide a thorough evaluation of all PV module cells. The overall status and longevity of the module can be determined at any stage[3].

Electroluminescence (EL) imaging is useful for fault detection and characterization in PV panels. As solar energy becomes more popular as a clean and sustainable power source, PV panel performance and longevity are crucial. Solar panel faults can be identified and classified noninvasively and efficiently using EL imaging, maximizing energy generation and maintenance. Images of solar cells' electroluminescent response to an electric field are captured using EL imaging. These images allow the detection of cracks, hotspots, and degradation patterns that may not be visible to the naked eye.

Some common fault types observed in EL images include cracks, i.e., visible breaks in solar cell structures, localized areas of high temperature, referred to as hotspots, and degradation patterns. This leads to reduced efficiency, resulting in diminished power output. By classifying these faults, technicians can identify the severity of the issue and take appropriate actions to rectify or mitigate its impact.

There are key challenges associated with fault classification. Manually inspecting and classifying faults in each panel is time-consuming and impractical as the number of solar panels in large-scale installations increases. Automating the classification process through the development of intelligent systems and algorithms is crucial for efficiently handling the volume of data generated by multiple panels. Thus, there is a need to create an automated classification system that can effectively categorize and differentiate between various fault types, which requires a deep understanding of the underlying physics and characteristics of each fault. Deep learning has emerged as a powerful data-driven approach for image classification applications because it can learn directly from a set of images. However, there are certain challenges associated with using deep learning for EL image classification. The limited spatial resolution, lack of color information, presence of noise and artifacts in images and limited spectral information are the major challenges associated with the use of deep learning for accurate classification.

There are many studies on EL imaging-based faulty panel identification. Overall, these methods can be categorized into traditional and machine learning algorithms. Several of the traditional methods include a logical gate-based image processing algorithm to enhance the crack regions [4], independent component analysis [5] and an anisotropic filter-based SVM approach for crack detection [6]. In this section, we review machine learning approaches. Zhang et al. [7] proposed a lightweight CNN with a size of 1.85 M learnable parameters based on the ResNet architecture for EL image classification. Based on the probability values, the overall set of images is divided into two classes, where panels are considered defective if their probability values are greater than 0.5. Their model achieved a maximum classification accuracy of 91.74%. In [8], the EL images were enhanced by equalizing the histogram of the images. Then, global information using the GCAM algorithm was integrated into an EfficientNet architecture to detect types of cracks or defects in the images. Attention-based deep learning was used in [9] to identify faulty panels from surface

images of panels and achieved 98.66% accuracy. An RGB dataset of panels with dust, cement, cracks, etc., are classified as faulty types in this research. The dataset contains dusty panel images that cannot be considered defective panels. In [10], the authors prepared their dataset using an OPT-M311 camera. They used image augmentation with rotation, brightness adaptation and mirror shifting. This dataset was used to train the CNN network. Their network performed well, with 98.40% accuracy. However, validation on open-source datasets was not presented in the paper. Rahman et al. [11] tested various pretrained CNN architectures, including VGG and its variant, ResNet50 variant and the Xception network, to identify defective panels from a set of images. In their experiment, they sorted images into three categories, i.e., uncracked, cracked and unsure, which are too distorted. Although unsure images have notation, due to large distortions, they differentiate them from a set of functional and defective images. The Inception V3 network achieved 96% accuracy on monocrystalline panels, and VGG16 achieved 91.2% accuracy on polycrystalline panels. The limitation of this work is that the overall accuracy of combining both methods was not presented in the paper.

This paper presents a low-complexity, resource-efficient deep convolution network for EL image classification. We modified the Xception network to classify EL images into two classes, i.e., normal or defective. The major challenges in EL images are their low resolution and lack of spectral information. The use of a depthwise separable convolution layer in the Xception network allows efficient modeling of spatial relations within images that capture both global and local features. Therefore, we modified an Xception network by reducing its learning parameters and providing efficient classification with a small dataset. The remainder of this paper is organized as follows: Section 2 presents the proposed modified Xception network for EL image classification. Section 3 discusses the dataset and results using the proposed network. Finally, a conclusion is established based on the experimental results.

Proposed Methodology

The deep neural network plays a vital role in image categorization. A wide variety of pretrained networks are available for use in image classification. However, the types of images are the key aspect of selecting the CNN network. As explained in Section 1, electroluminescence imaging is a better choice for detecting faults within the cell of a PV module. However, the lack of spectral information and resolution makes this process challenging. A traditional CNN applies a set of filters K to the input feature map X with dimensions H × W × C, where H represents the height, W represents the width, and C represents the number of input channels. For the EL images, C is 1. Each filter has dimensions F x F x C, where F represents the filter size. The convolution operation is performed by sliding each filter across the input feature map, computing the elementwise multiplication between the filter and the corresponding spatial region of the input, and summing the results to produce an output feature map.

The Xception network modifies this convolutional operation by separating the spatial and channelwise information. It introduces two separate convolutional operations: depthwise convolution and pointwise convolution. The depthwise convolution operates on each input channel independently. It applies a set of depthwise filters, denoted as K_d, to each input channel of the feature map X. The depthwise filters have dimensions F × F × 1, where 1 represents the number of input channels. The depthwise convolution produces a set of intermediate feature maps, denoted as M, with dimensions H x W. Mathematically, the depthwise convolution can be represented as:

$$M = \text{DepthwiseConv}(X, K_d) \quad (1)$$

The pointwise convolution performs a 1x1 convolution on the intermediate feature maps M obtained from the depthwise convolution. It applies a set of pointwise filters, denoted as K_p, to combine and transform the intermediate feature maps. The pointwise filters have dimensions of 1 x 1 x C', where C' represents the number of output channels. The pointwise convolution produces

the final output feature map, denoted as Y, with dimensions H x W x C'. Mathematically, it can be represented as:

$$Y = \text{PointwiseConv}(M, K_p) \quad (2)$$

By separating the spatial and channelwise convolutions, the Xception network reduces the number of parameters and computations compared to standard convolutions. This parameter efficiency makes the Xception network computationally efficient and suitable for deep learning tasks with limited computational resources. The Xception network architecture repeats the depthwise and pointwise convolutions in multiple layers, enabling the network to learn hierarchical representations of features at different scales and complexities. Additionally, the Xception network often incorporates other common components found in deep neural networks, such as pooling layers, activation functions, and fully connected layers, to further enhance its performance. The structure of the Xception network, shown in Figure 1, is established based on the experimental results.

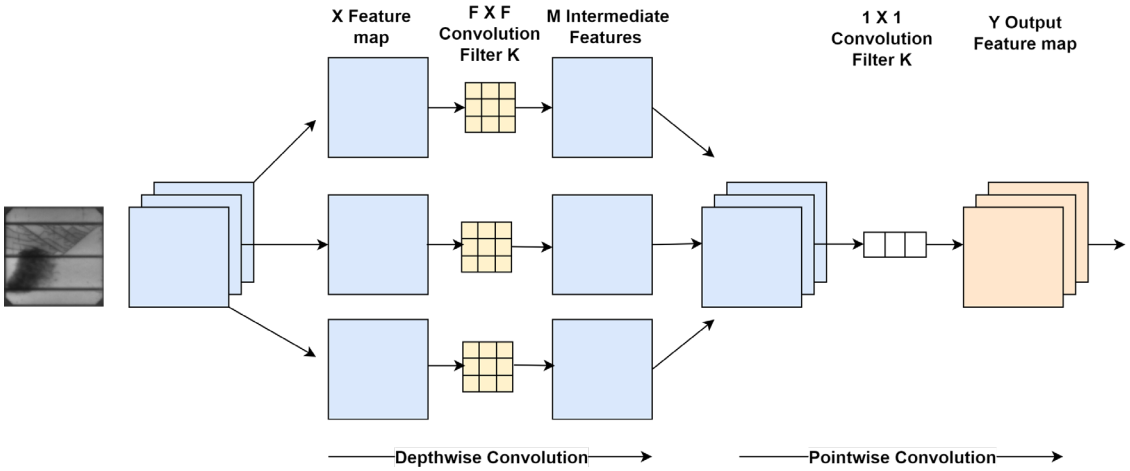

Figure 1 Xception network structure for convolution operation

The Xception network is built using stacking depth-separable convolution and comprises 14 modules, each with 36 convolutional layers. All of the layers utilize this technique except for the first 2 and the ones linked by residuals; the basic network is also built using this method. The pretrained Xception network has 170 deep layers with 22.9 million learnable parameters. The internal structure represented in Figure 2 is repeated 12 times with additional separable convolution layers in a few of the blocks. Here, this network is modified to classify grayscale EL images. In the proposed network, the initial layer is modified for grayscale images. The initial 80 layers of the pretrained Xception network are the same as those of the proposed network. The size of the network is reduced by removing the last four blocks. In addition, dropout layers are added to block 7 and the last block of the structure to reduce the feature size. These dropout layers help to solve the problem of network overfitting. The overall proposed structure has 120 layers with 14.3 M learnable parameters.

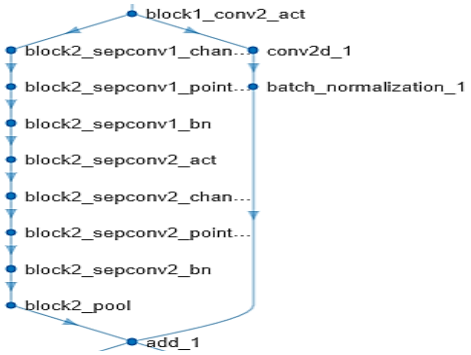

Figure 2 One block of convolution operations in the Xception network

Result Analysis and Discussion

Dataset

There is a wide variety of PV cell faults; however, not all of them will cause a significant drop in power output. The power output of the module is unaffected by some flaws, but it can be reduced over time, or the cells can disengage from the module due to others [12]. EL imaging can reveal cracks, microcracks, fractures, disconnections, silicone material flaws, finger disruptions, and unconnected cells. In this study, overall, PV cells were classified into two categories, i.e., normal and defective, if the panel had any of the above abnormalities. The ELVP dataset prepared using 18 monocrystalline and 26 polycrystalline PV panels from [13] was used in the experiments. A total of 2624 EL solar cell images, including 1508 normal images and 1116 defective images, are available in this dataset. Out of 1116 defective images, 715 images are faulty with 100% probability, and the remaining images have a lower probability of being faulty. Therefore, in the experiment, we used 1508 normal images and 716 defective images. We divided the EL images into a training set consisting of 80% (1206 normal and 573 defective) and a test set consisting of 20% for dataset partitioning. The sample images of both the normal and defective panels are shown in Figure 3.

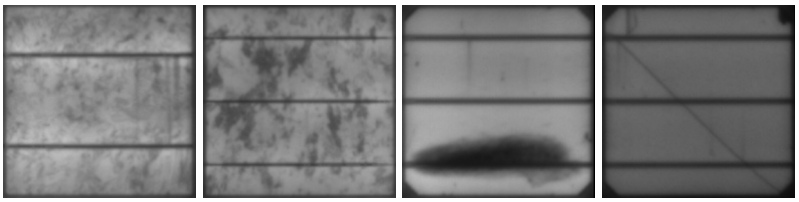

Figure 3 Sample images from the dataset (the left two images are normal panels, and the right two images are defective panels)

The small size of the dataset causes overfitting. Therefore, before using this dataset, an augmentation of images is used to enlarge the dataset. The dataset used had perfectly aligned EL images. Therefore, during the augmentation process, rotations of 90° and 180° were used. In addition, random shifting in both the X-direction and Y-direction is performed by increasing the set of training and testing images. This also helps to address the imbalance between the two classes.

Results and Discussion

The ADAM optimizer is used in a modified Xception network. The learning rate is initialized to 0.0001. The maximum number of epochs used is 10, and 64 is selected for the mini-batch size. Images are shuffled at every epoch for better network performance. We decided to quantify the classification effect and performance of our suggested model using accuracy, recall, precision, and F1 score, which are four commonly used metrics for evaluating and comparing effective models. In particular, higher values indicate better results for F1, recall, accuracy, and precision. If true positives (TPs) and true negatives (TNs) represent the number of positive results, for example, corrected detection of normal and defective panels, whereas false positives (FPs) and false negatives (FNs) represent the number of negative results, then these matrices can be calculated as follows:

$$Precision = \frac{TP}{TP+FP}, \qquad Recall = \frac{TP}{TP+FN} \tag{3}$$

$$Accuracy = \frac{TP+TN}{TP+TN+FP+FN} \qquad F1-Score = \frac{2 \times Precision \times Recall}{Precision+Recall} \tag{4}$$

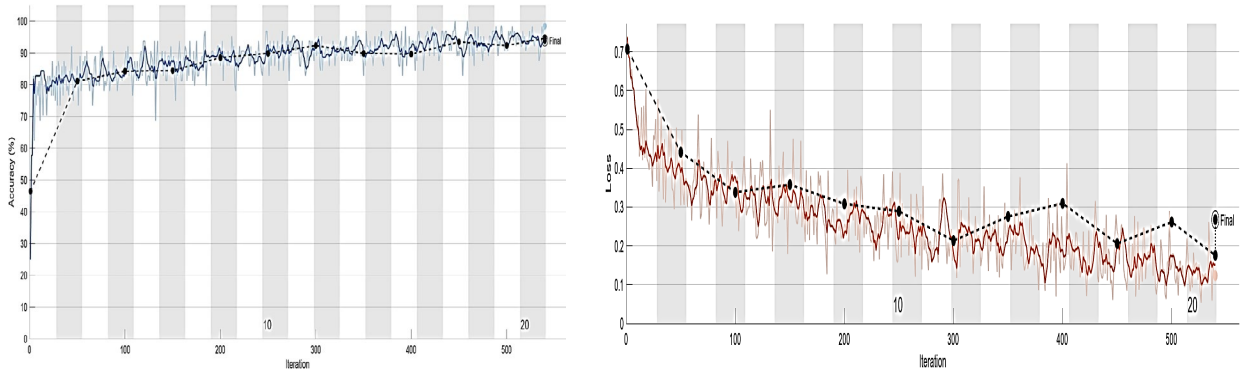

Figure 4 Accuracy and loss variation over time for the training and test datasets

The normal PV cell EL images had a uniform surface, but they had shadowed areas or impurities in the background. The backgrounds were clear and textured, but they were not defective; this put some pressure on the model to find defects. It was challenging to differentiate the surface defects of aberrant PV cells from the background in the EL image because they looked so similar to the background in the original image. The accuracy and loss analysis over the epochs for the training dataset are shown in Figure 4. Figure 4 shows that the model succeeded in achieving 93.93% accuracy with a training loss of less than 0.2.

The confusion matrix represents the TP, TN, FP and FN results of the network. Figure 5 shows the confusion matrix of the proposed network for the training dataset.

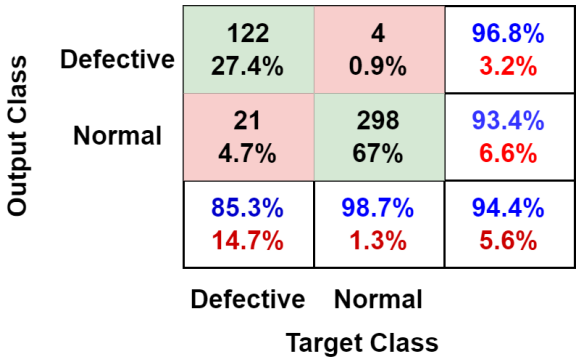

Figure 5 Confusion matrix of the modified Xception network

In Figure 5, the first two diagonal cells show the number and percentage of correct classifications by the network. For example, 122-panel images are correctly classified as defective. This corresponds to 27.4% of all test set images. Similarly, 298 cases are correctly classified as normal. This corresponds to 67% of all test images. Twenty-one of the defective panels are incorrectly classified as normal, which corresponds to 4.7% of all images. Out of 302 normal test images, 98.7% are correct and 1.3% are incorrect. Overall, 94.4% of the predictions are correct, and 5.6% are wrong.

Some of the most successful approaches to PV defect detection in the past few years were compared to our model. We selected these approaches for testing and assessment on the same dataset as our proposed model to ensure a fair comparison; Table 1 displays the results of the method comparison.

Table 1 Comparison of the experimental results with those of other methods

Model	Accuracy	Precision	Recall	F1 Score
CNN [14]	78.38	77.86	70.10	71.84
VGG16 [14]	84.01	82.26	80.31	81.15
InceptionV3 [14]	88.96	87.73	86.72	87.20
SVM [15]	82.44	-	-	85.52
CNN [15]	88.42	-	-	88.39
L-CNN [16]	89.33	90.44	95.42	92.86
Our network	94.382	92	95.12	93.53

As shown in Table 1, pretrained networks, including CNN, VGG16 and InceptionV3, were tested in [14], and their models were compared. The presence of noise makes it challenging, and therefore, these models struggle to classify faulty panels from the set of images. In [15], the authors extracted various VGG-based CNN features, and SVM was used as a classifier. A validation of the experiment using mono-, poly- and the overall set of images was presented in the paper. However, their accuracy was limited to 88.42 max when using a CNN. In [16], a lightweight convolutional neural network was presented. They trained it from scratch, and a comparison with a support vector machine was presented in their work. Their light CNN succeeded at 89.33% accuracy for two-class classification. In contrast, the modification of the Xception network with the removal of a few separable convolution layers and the introduction of dropout layers performed well on augmented images and achieved 90% accuracy.

Conclusion

Solar cells have crystal grain boundaries due to the intrinsic silicon structure, and the presence of noise in EL images causes ambiguity in distinguishing minor cracks. In addition, EL images lack spectral information. These characterizations impose a challenge to applying conventional CNN networks to identify faulty cells from normal cells. In this paper, we used the Xception network to determine whether a panel is defective. The large number of layers in deep CNNs increases the complexity of the network; hence, the network cannot learn well from grayscale images. Therefore, the network is minimized by removing repetitive separable convolution layers. Furthermore, dropout layers are introduced in the Xception network to solve the overfitting problem, and the experimental results and a comparison with state-of-the-art methods suggest that the model's classification accuracy is improved. The experimental results are validated for binary classification only. Therefore, further validation of the network for multiclass classification will be performed in the future.

References

[1] W. Tang, Q. Yang, K. Xiong, and W. Yan, "Deep learning based automatic defect identification of photovoltaic module using electroluminescence images," *Solar Energy*, vol. 201, pp. 453–460, May 2020. https://doi.org/10.1016/j.solener.2020.03.049

[2] M. W. Akram *et al.*, "CNN based automatic detection of photovoltaic cell defects in electroluminescence images," *Energy*, vol. 189, p. 116319, Dec. 2019.

[3] U. Jahn, M. Herz, M. Köntges, D. Parlevliet, M. Paggi, and I. Tsanakas, *Review on infrared and electroluminescence imaging for PV field applications: International Energy Agency Photovoltaic Power Systems Programme: IEA PVPS Task 13, Subtask 3.3: report IEA-PVPS T13-12:2018*. Paris: International Energy Agency, 2018.

[4] M. Dhimish, V. Holmes, and P. Mather, "Novel Photovoltaic Micro Crack Detection Technique," *IEEE Trans. Device Mater. Relib.*, vol. 19, no. 2, pp. 304–312, Jun. 2019. https://doi.org/10.1109/TDMR.2019.2907019

[5] D.-M. Tsai, S.-C. Wu, and W.-Y. Chiu, "Defect Detection in Solar Modules Using ICA Basis Images," *IEEE Trans. Ind. Inf.*, vol. 9, no. 1, pp. 122–131, Feb. 2013. https://doi.org/10.1109/TII.2012.2209663

[6] S. A. Anwar and M. Z. Abdullah, "Micro-crack detection of multicrystalline solar cells featuring an improved anisotropic diffusion filter and image segmentation technique," *J Image Video Proc*, vol. 2014, no. 1, p. 15, Dec. 2014. https://doi.org/10.1186/1687-5281-2014-15

[7] J. Zhang, X. Chen, H. Wei, and K. Zhang, "A lightweight network for photovoltaic cell defect detection in electroluminescence images based on neural architecture search and knowledge distillation," *Applied Energy*, vol. 355, p. 122184, Feb. 2024.

[8] Q. Liu, M. Liu, C. Wang, and Q. M. J. Wu, "An efficient CNN-based detector for photovoltaic module cells defect detection in electroluminescence images," *Solar Energy*, vol. 267, p. 112245, Jan. 2024. https://doi.org/10.1016/j.solener.2023.112245

[9] D. Dwivedi, K. V. S. M. Babu, P. K. Yemula, P. Chakraborty, and M. Pal, "Identification of surface defects on solar PV panels and wind turbine blades using attention based deep learning model," *Engineering Applications of Artificial Intelligence*, vol. 131, p. 107836, May 2024. https://doi.org/10.1016/j.engappai.2023.107836

[10] M. Sun, S. Lv, X. Zhao, R. Li, W. Zhang, and X. Zhang, "Defect Detection of Photovoltaic Modules Based on Convolutional Neural Network," in *Machine Learning and Intelligent Communications*, vol. 226, X. Gu, G. Liu, and B. Li, Eds., in Lecture Notes of the Institute for Computer Sciences, Social Informatics and Telecommunications Engineering, vol. 226. , Cham: Springer International Publishing, 2018, pp. 122–132. https:/10.1007/978-3-319-73564-1_13

[11] Md. R. Rahman, S. Tabassum, E. Haque, M. M. Nishat, F. Faisal, and E. Hossain, "CNN-based Deep Learning Approach for Micro-crack Detection of Solar Panels," in *2021 3rd International Conference on Sustainable Technologies for Industry 4.0 (STI)*, Dhaka, Bangladesh: IEEE, Dec. 2021, pp. 1–6. doi: 10.1109/STI53101.2021.9732592

[12] M. Köntges, S. Kurtz, C. Packard, U. Jahn, K. A. Berger, and K. Kato, *Performance and reliability of photovoltaic systems: subtask 3.2: Review of failures of photovoltaic modules: IEA PVPS task 13: external final report IEA-PVPS*. Sankt Ursen: International Energy Agency, Photovoltaic Power Systems Programme, 2014.

[13] L. Pratt, J. Mattheus, and R. Klein, "A benchmark dataset for defect detection and classification in electroluminescence images of PV modules using semantic segmentation," *Systems and Soft Computing*, vol. 5, p. 200048, Dec. 2023. https://doi.org/10.1016/j.sasc.2023.200048

[14] J. Wang *et al.*, "Deep-Learning-Based Automatic Detection of Photovoltaic Cell Defects in Electroluminescence Images," *Sensors*, vol. 23, no. 1, p. 297, Dec. 2022. https://doi.org/10.3390/s23010297

[15] S. Deitsch *et al.*, "Automatic classification of defective photovoltaic module cells in electroluminescence images," *Solar Energy*, vol. 185, pp. 455–468, Jun. 2019. https://doi.org/10.1016/j.solener.2019.02.067

[16] M. Y. Demirci, N. Beşli, and A. Gümüşçü, "Efficient deep feature extraction and classification for identifying defective photovoltaic module cells in Electroluminescence images," *Expert Systems with Applications*, vol. 175, p. 114810, Aug. 2021. https://doi.org/10.1016/j.eswa.2021.114810